arXiv:0802.2499v2 [hep-ex] 22 May 2008

Measurement of Azimuthal Asymmetries With Respect To Both Beam Charge and Transverse Target Polarization in Exclusive Electroproduction of Real Photons

HERMES Collaboration

A. Airapetian[15], N. Akopov[26], Z. Akopov[26], A. Andrus[14], E.C. Aschenauer[6], W. Augustyniak[25], R. Avakian[26], A. Avetissian[26], E. Avetisyan[5,10], L. Barion[9], S. Belostotski[18], N. Bianchi[10], H.P. Blok[17,24], H. Böttcher[6], C. Bonomo[9], A. Borissov[13], A. Brüll[27], V. Bryzgalov[19], J. Burns[13], M. Capiluppi[9], G.P. Capitani[10], E. Cisbani[21], G. Ciullo[9], M. Contalbrigo[9], P.F. Dalpiaz[9], W. Deconinck[15], R. De Leo[2], M. Demey[17], L. De Nardo[5,22], E. De Sanctis[10], M. Diefenthaler[8], P. Di Nezza[10], J. Dreschler[17], M. Düren[12], M. Ehrenfried[12], G. Elbakian[26], F. Ellinghaus[4], U. Elschenbroich[11], R. Fabbri[6], A. Fantoni[10], L. Felawka[22], S. Frullani[21], A. Funel[10], D. Gabbert[6], G. Gapienko[19], V. Gapienko[19], F. Garibaldi[21], G. Gavrilov[5,18,22], V. Gharibyan[26], F. Giordano[9], S. Gliske[15], H. Guler[6], C. Hadjidakis[10], D. Hasch[10], T. Hasegawa[23], G. Hill[13], A. Hillenbrand[8], M. Hoek[13], Y. Holler[5], I. Hristova[6], G. Iarygin[7], Y. Imazu[23], A. Ivanilov[19], A. Izotov[18], H.E. Jackson[1], A. Jgoun[18], S. Joosten[11], R. Kaiser[13], T. Keri[12], E. Kinney[4], A. Kisselev[14,18], M. Kopytin[6], V. Korotkov[19], V. Kozlov[16], P. Kravchenko[18], V.G. Krivokhijine[7], L. Lagamba[2], R. Lamb[14], L. Lapikás[17], I. Lehmann[13], P. Lenisa[9], L.A. Linden-Levy[14], W. Lorenzon[15], S. Lu[12], X. Lu[23], B.-Q. Ma[3], D. Mahon[13], B. Maiheu[11], N.C.R. Makins[14], Y. Mao[3], B. Marianski[25], H. Marukyan[26], C.A. Miller[22], Y. Miyachi[23], V. Muccifora[10], M. Murray[13], A. Mussgiller[8], A. Nagaitsev[7], E. Nappi[2], Y. Naryshkin[18], A. Nass[8], M. Negodaev[6], W.-D. Nowak[6], A. Osborne[13], L.L. Pappalardo[9], R. Perez-Benito[12], N. Pickert[8], M. Raithel[8], P.E. Reimer[1], A. Reischl[17], A.R. Reolon[10], C. Riedl[10], K. Rith[8], S.E. Rock[5], G. Rosner[13], A. Rostomyan[5], L. Rubacek[12], J. Rubin[14], A.L. Ruiz[11], D. Ryckbosch[11], Y. Salomatin[19], I. Sanjiev[1,18], A. Schäfer[20], G. Schnell[11], K.P. Schüler[5], B. Seitz[13],

C.Shearer[13], T.-A. Shibata[23], V. Shutov[7], M. Stancari[9], M. Statera[9], E. Steffens[8], J.J.M. Steijger[17], H. Stenzel[12], J. Stewart[6], F. Stinzing[8], P. Tait[8], S. Taroian[26], A. Terkulov[16], A. Trzcinski[25], M. Tytgat[11], A. Vandenbroucke[11], P.B. van der Nat[17], G. van der Steenhoven[17], Y. Van Haarlem[11], C. Van Hulse[11], M. Varanda[5], D. Veretennikov[18], V. Vikhrov[18], I. Vilardi[2], C. Vogel[8], S. Wang[3], S. Yaschenko[8], H. Ye[3], Z. Ye[5], S. Yen[22], W. Yu[12], D. Zeiler[8], B. Zihlmann[11] and P. Zupranski[25].

[1]Physics Division, Argonne National Laboratory, Argonne, Illinois 60439-4843, USA
[2]Istituto Nazionale di Fisica Nucleare, Sezione di Bari, 70124 Bari, Italy
[3]School of Physics, Peking University, Beijing 100871, China
[4]Nuclear Physics Laboratory, University of Colorado, Boulder, Colorado 80309-0390, USA
[5]DESY, 22603 Hamburg, Germany
[6]DESY, 15738 Zeuthen, Germany
[7]Joint Institute for Nuclear Research, 141980 Dubna, Russia
[8]Physikalisches Institut, Universität Erlangen-Nürnberg, 91058 Erlangen, Germany
[9]Istituto Nazionale di Fisica Nucleare, Sezione di Ferrara and Dipartimento di Fisica, Università di Ferrara, 44100 Ferrara, Italy
[10]Istituto Nazionale di Fisica Nucleare, Laboratori Nazionali di Frascati, 00044 Frascati, Italy
[11]Department of Subatomic and Radiation Physics, University of Gent, 9000 Gent, Belgium
[12]Physikalisches Institut, Universität Gießen, 35392 Gießen, Germany
[13]Department of Physics and Astronomy, University of Glasgow, Glasgow G12 8QQ, United Kingdom
[14]Department of Physics, University of Illinois, Urbana, Illinois 61801-3080, USA
[15]Randall Laboratory of Physics, University of Michigan, Ann Arbor, Michigan 48109-1040, USA
[16]Lebedev Physical Institute, 117924 Moscow, Russia
[17]Nationaal Instituut voor subatomaire fysica (Nikhef), 1009 DB Amsterdam, The Netherlands
[18]Petersburg Nuclear Physics Institute, St. Petersburg, Gatchina, 188350 Russia
[19]Institute for High Energy Physics, Protvino, Moscow region, 142281 Russia
[20]Institut für Theoretische Physik, Universität Regensburg, 93040 Regensburg, Germany
[21]Istituto Nazionale di Fisica Nucleare, Sezione Roma 1, Gruppo Sanità and Physics Laboratory, Istituto Superiore di Sanità, 00161 Roma, Italy
[22]TRIUMF, Vancouver, British Columbia V6T 2A3, Canada
[23]Department of Physics, Tokyo Institute of Technology, Tokyo 152, Japan
[24]Department of Physics and Astronomy, Vrije Universiteit, 1081 HV Amsterdam, The Netherlands
[25]Andrzej Soltan Institute for Nuclear Studies, 00-689 Warsaw, Poland
[26]Yerevan Physics Institute, 375036 Yerevan, Armenia
[27]Present address: 36 Mizzen Circle, Hampton, Virginia 23664, USA

E-mail: *management@hermes.desy.de*

Abstract. Azimuthal asymmetries in exclusive electroproduction of real photons are measured for the first time with respect to transverse target polarisation, providing new constraints on Generalized Parton Distributions. From the same data set on a hydrogen target, new results for the beam-charge asymmetry are also extracted with better precision than those previously reported. By comparing model calculations with measured asymmetries attributed to the interference between the deeply virtual Compton scattering and Bethe-Heitler processes, a model-dependent constraint is obtained on the total angular momenta carried by up and down quarks in the nucleon.

PACS numbers: 13.60.-r 24.85.+p 13.60.Fz 14.20.Dh

1. Introduction

The partonic structure of the nucleon has traditionally been described in terms of Parton Distribution Functions (PDFs) of the parton's longitudinal momentum as a fraction of the nucleon's momentum in a frame in which the nucleon is moving at almost the velocity of light. These functions appear in the theoretical description of, e.g., Deep-Inelastic Scattering (DIS). However, in the context of the rapid theoretical developments of the last decade, PDFs have been conceptually subsumed within the broader framework of Generalized Parton Distributions (GPDs), which also describe elastic form factors and amplitudes for hard-exclusive reactions leaving the target nucleon intact [1, 2, 3]. Most often discussed are the four twist-2 quark-chirality conserving quark GPDs: the polarisation-independent distributions H_q and E_q and the polarisation-dependent distributions $\widetilde{H}_q$ and $\widetilde{E}_q$. The GPDs H_q and $\widetilde{H}_q$ conserve nucleon helicity, while E_q and $\widetilde{E}_q$ are associated with a helicity flip of the nucleon. GPDs depend on the kinematic variables x and ξ, which represent respectively the average and difference of the longitudinal momentum fractions of the probed parton in the initial and final states. The variable ξ is typically nonzero in hard-exclusive reactions. GPDs also depend on the squared four-momentum transfer $t = (p - p')^2$ to the nucleon, with p (p') the four-momentum of the nucleon in the initial (final) state. PDFs and nucleon elastic form factors appear as kinematic limits ($t \to 0$) and x-moments of GPDs, respectively. Strong interest in the formalism of GPDs and their experimental constraint has emerged after moments of certain GPDs were found to relate directly to the total (including orbital) angular momenta carried by partons in the nucleon, via the Ji relation [2]:

$$\lim_{t\to 0} \int_0^1 \mathrm{d}x \; x \left(H_q(x,\xi,t) + E_q(x,\xi,t)\right) = J_q \tag{1}$$

This finding offers for the first time a path towards solving the 'nucleon spin puzzle' of how the helicities and orbital angular momenta of quarks and gluons combine to form the spin of the nucleon. More recent discussions have focused on the potential of GPDs as multi-dimensional representations of hadrons at the partonic level, correlating the longitudinal momentum fraction with transverse spatial coordinates [4, 5, 6, 7, 8].

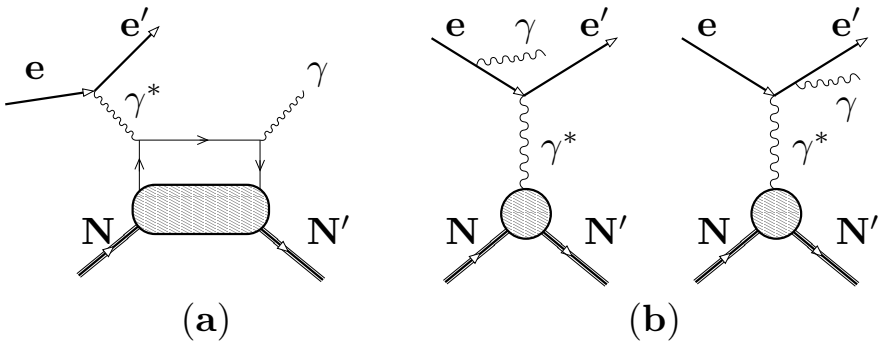

Figure 1. Leading-order diagrams for (a) deeply virtual Compton scattering (handbag diagram) and (b) Bethe-Heitler processes.

2. Deeply virtual Compton scattering

Generalized Parton Distributions are accessible through exclusive processes that involve at least two hard vertices, yet leave the target nucleon intact. Among all presently practical hard exclusive probes, the Deeply Virtual Compton Scattering (DVCS) process, i.e., the hard exclusive leptoproduction of a real photon (e.g., $\gamma^* N \to \gamma N'$), appears to have the most reliable interpretation in terms of GPDs. In electroproduction, direct access to the DVCS amplitude $\mathrm{T_{DVCS}}$ is provided by the interference between the DVCS and Bethe-Heitler (BH) processes, in which the photon is radiated from a quark and from the lepton, respectively (see Fig. 1). Since these processes are intrinsically indistinguishable, the cross section is proportional to the squared photon-production amplitude written as

$$|\mathrm{T}|^2 = |\mathrm{T_{DVCS}}|^2 + |\mathrm{T_{BH}}|^2 + \underbrace{\mathrm{T_{DVCS}}\mathrm{T^*_{BH}} + \mathrm{T^*_{DVCS}}\mathrm{T_{BH}}}_{\mathrm{I}}, \tag{2}$$

where 'I' denotes the interference term. The BH amplitude $\mathrm{T_{BH}}$ is precisely calculable from measured elastic form factors of the nucleon and provides the dominant contribution in Eq. 2 in the kinematic conditions of the present measurement. These amplitudes depend on $Q^2 = -q^2$ with $q = k - k'$ and k (k') the four-momentum of the lepton in the initial (final) state, the variable $x_B = Q^2/(2M\nu)$ with $\nu = p \cdot q/M$ and M the nucleon mass, and t. In addition, the amplitudes depend on ϕ and, in the case of a target polarisation component orthogonal to $\vec{q}$, on ϕ_S, the azimuthal angles about the virtual-photon direction that are defined in Fig. 2. The dependences on ϕ related to beam helicity and beam charge have been investigated experimentally [9, 10, 11, 12], resulting in first constraints on GPDs.

At Leading Order (LO) in the fine-structure constant α_{em}, the squared BH amplitude $|\mathrm{T_{BH}}|^2$ is independent of the target polarisation with an unpolarised beam, and independent of the lepton charge. In contrast, the squared DVCS amplitude $|\mathrm{T_{DVCS}}|^2$ and the interference term I can depend on the target polarisation even with an unpolarised beam, and the sign of the interference term depends also on the lepton

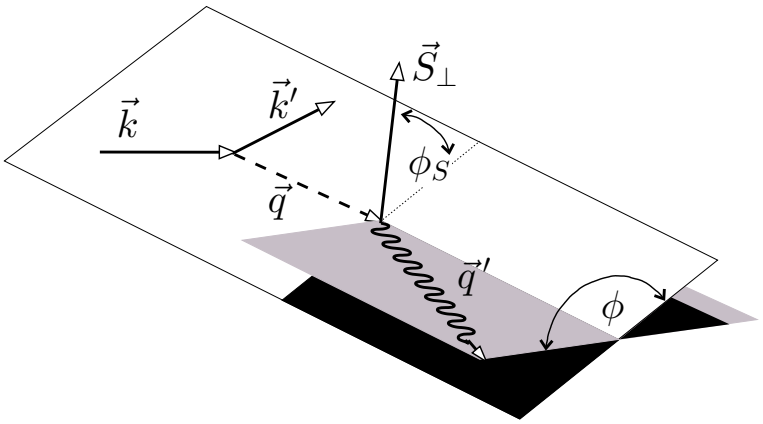

Figure 2. Momenta and azimuthal angles for exclusive electroproduction of photons in the target rest frame. The quantity ϕ denotes the angle between the lepton plane containing the three-momenta $\vec{k}$ and $\vec{k}'$ of the incoming and outgoing lepton and the plane correspondingly defined by $\vec{q} = \vec{k} - \vec{k}'$ and the momentum $\vec{q}'$ of the real photon. The symbol ϕ_S denotes the angle between the lepton plane and $\vec{S}_\perp$, the component of the target polarisation vector that is orthogonal to $\vec{q}$. These definitions are consistent with the Trento conventions [13].

charge. For an unpolarised lepton beam and a transversely polarised nucleon target, these dependences read [14, 15]

$$|\mathrm{T}_{BH}|^2 = \frac{K_{\mathrm{BH}}}{\mathcal{P}_1(\phi)\mathcal{P}_2(\phi)}\Big(c^{\mathrm{BH}}_{0,\mathrm{UU}} + \Big\{c^{\mathrm{BH}}_{1,\mathrm{UU}}\cos\phi + \big\{c^{\mathrm{BH}}_{2,\mathrm{UU}}\cos(2\phi)\big\}\Big\}\Big), \tag{3}$$

$$\begin{aligned}|\mathrm{T}_{DVCS}|^2 &= K_{\mathrm{DVCS}}\Big(c^{\mathrm{DVCS}}_{0,\mathrm{UU}} + c^{\mathrm{DVCS}}_{2,\mathrm{UU}}\cos(2\phi) + \big\{c^{\mathrm{DVCS}}_{1,\mathrm{UU}}\cos\phi\big\} \\ &\quad + S_\perp\Big[\boldsymbol{c^{\mathrm{DVCS}}_{0,\mathrm{UT}}\sin(\phi-\phi_S)} + c^{\mathrm{DVCS}}_{2,\mathrm{UT}}\sin(\phi-\phi_S)\cos(2\phi) \\ &\quad + s^{\mathrm{DVCS}}_{2,\mathrm{UT}}\cos(\phi-\phi_S)\sin(2\phi) \\ &\quad + \big\{c^{\mathrm{DVCS}}_{1,\mathrm{UT}}\sin(\phi-\phi_S)\cos\phi + s^{\mathrm{DVCS}}_{1,\mathrm{UT}}\cos(\phi-\phi_S)\sin\phi\big\}\Big]\Big),\end{aligned} \tag{4}$$

$$\begin{aligned}\mathrm{I} &= \frac{-K_{\mathrm{I}}e_l}{\mathcal{P}_1(\phi)\mathcal{P}_2(\phi)}\Big(\boldsymbol{c^{\mathrm{I}}_{1,\mathrm{UU}}\cos\phi} + c^{\mathrm{I}}_{3,\mathrm{UU}}\cos(3\phi) \\ &\quad + \big\{\boldsymbol{c^{\mathrm{I}}_{0,\mathrm{UU}}} + c^{\mathrm{I}}_{2,\mathrm{UU}}\cos(2\phi)\big\} \\ &\quad + S_\perp\Big[\boldsymbol{c^{\mathrm{I}}_{1,\mathrm{UT}}\sin(\phi-\phi_S)\cos\phi + s^{\mathrm{I}}_{1,\mathrm{UT}}\cos(\phi-\phi_S)\sin\phi} \\ &\quad + c^{\mathrm{I}}_{3,\mathrm{UT}}\sin(\phi-\phi_S)\cos(3\phi) + s^{\mathrm{I}}_{3,\mathrm{UT}}\cos(\phi-\phi_S)\sin(3\phi) \\ &\quad + \big\{\boldsymbol{c^{\mathrm{I}}_{0,\mathrm{UT}}\sin(\phi-\phi_S)} + c^{\mathrm{I}}_{2,\mathrm{UT}}\sin(\phi-\phi_S)\cos(2\phi) \\ &\quad + s^{\mathrm{I}}_{2,\mathrm{UT}}\cos(\phi-\phi_S)\sin(2\phi)\big\}\Big]\Big).\end{aligned} \tag{5}$$

Here, $S_\perp$ denotes the magnitude of the transverse target polarisation, e_l the beam charge in units of the elementary charge, $\mathcal{P}_1(\phi)\mathcal{P}_2(\phi)$ contains the ϕ-dependent lepton propagators, and the braces enclose terms that are kinematically suppressed by $1/Q$. The subscripts 'UU' and 'UT' denote an unpolarised beam with unpolarised and transversely polarised targets, respectively. The dependences of the coefficients c_n

and s_n on GPDs are elaborated in Ref. [15], where the kinematic factors K are defined. The factor $K_{\rm DVCS}$ in Eq. 4 suppresses the squared DVCS amplitude by two orders of magnitude relative to the interference term in the kinematics of the present measurement. Note that the azimuthal angles defined here are different from those used in Ref. [15] ($\phi = \pi - \phi_{[15]}$ and $\phi - \phi_s = \pi + \varphi_{[15]}$), leading to opposite signs for some of the coefficients given below.

The terms of particular interest in this paper appear in bold face in Eqs. 4 and 5. The corresponding coefficients can be approximated as

$$c_{0,\rm UT}^{\rm DVCS} \propto -\frac{\sqrt{-t}}{M}{\rm Im}\left\{\boldsymbol{\mathcal{H}\mathcal{E}^*} - \boldsymbol{\mathcal{E}\mathcal{H}^*} + \boldsymbol{\xi\widetilde{\mathcal{E}}\,\widetilde{\mathcal{H}}^*} - \boldsymbol{\widetilde{\mathcal{H}}\,\xi\widetilde{\mathcal{E}}^*}\right\}, \tag{6}$$

$$c_{1,\rm UU}^{\rm I} \propto \frac{\sqrt{-t}}{Q}{\rm Re}\left\{\boldsymbol{F_1\mathcal{H}} + \xi(F_1+F_2)\widetilde{\mathcal{H}} - \frac{t}{4M^2}F_2\mathcal{E}\right\}, \tag{7}$$

$$c_{0,\rm UU}^{\rm I} \propto -\frac{\sqrt{-t}}{Q}c_{1,\rm UU}^{\rm I}, \tag{8}$$

$$\begin{aligned} c_{1,\rm UT}^{\rm I} \propto -\frac{M}{Q}{\rm Im}\Bigg\{&\frac{\boldsymbol{t}}{\boldsymbol{4M^2}}\left[\boldsymbol{(2-x_B)F_1\mathcal{E}} - 4\frac{\boldsymbol{1-x_B}}{\boldsymbol{2-x_B}}\boldsymbol{F_2\mathcal{H}}\right] \\ &+x_B\xi\left[F_1(\mathcal{H}+\mathcal{E}) - (F_1+F_2)(\widetilde{\mathcal{H}} + \frac{t}{4M^2}\widetilde{\mathcal{E}})\right]\Bigg\}, \end{aligned} \tag{9}$$

$$c_{0,\rm UT}^{\rm I} \propto -\frac{\sqrt{-t}}{Q}c_{1,\rm UT}^{\rm I}, \tag{10}$$

$$\begin{aligned} s_{1,\rm UT}^{\rm I} \propto -\frac{M}{Q}{\rm Im}\Bigg\{&\frac{\boldsymbol{t}}{\boldsymbol{4M^2}}\left[4\frac{\boldsymbol{1-x_B}}{\boldsymbol{2-x_B}}\boldsymbol{F_2\widetilde{\mathcal{H}}} - \boldsymbol{(F_1+\xi F_2)x_B\widetilde{\mathcal{E}}}\right] \\ &+ x_B\left[(F_1+F_2)\left(\xi\mathcal{H} + \frac{t}{4M^2}\mathcal{E}\right) - \xi F_1(\widetilde{\mathcal{H}} + \frac{x_B}{2}\widetilde{\mathcal{E}})\right]\Bigg\}, \end{aligned} \tag{11}$$

with the skewness ξ approximated by $\xi \approx x_B/(2-x_B)$. The Compton form factors $\mathcal{H}$, $\mathcal{E}$, $\widetilde{\mathcal{H}}$ and $\widetilde{\mathcal{E}}$ are convolutions of hard scattering amplitudes with the corresponding twist-two quark GPDs H_q, E_q, $\widetilde{H}_q$ and $\widetilde{E}_q$, while F_1 and F_2 are the nucleon Dirac and Pauli form factors [15]. In Eqs. 6-11, the use of bold face differs from that in Eqs. 4 and 5. Here, the terms not in bold face are suppressed relative to those in bold face in the same equation by either x_B (or ξ) or t/M^2, which are of order 0.1 in the kinematic conditions of this measurement. The terms containing $x_B\widetilde{\mathcal{E}}$ (or $\xi\widetilde{\mathcal{E}}$) are not suppressed because the pion-pole contribution to $\widetilde{E}$ scales as $1/x_B$.

The coefficients $c_{0,\rm UU}^{\rm I}$ and $c_{1,\rm UU}^{\rm I}$ provide an experimental constraint on the real part of the Compton form factors, and can be used to test various models for GPDs as in Ref. [12]. Most importantly for the present work, the coefficients $c_{0,\rm UT}^{\rm DVCS}$, $c_{0,\rm UT}^{\rm I}$ and $c_{1,\rm UT}^{\rm I}$ provide rare access to the GPD E with no kinematic suppression of its contribution relative to those of the other GPDs. Measurements sensitive to these coefficients may provide via the Ji relation (Eq. 1) an opportunity to constrain parameterisations of the GPD E_q in terms of J_q [16]. The coefficient $c_{0,\rm UU}^{\rm I}$ ($c_{0,\rm UT}^{\rm I}$) has approximately the same dependence on GPDs as $c_{1,\rm UU}^{\rm I}$ ($c_{1,\rm UT}^{\rm I}$). The apparent overall suppression of $c_{0,\rm UU}^{\rm I}$ and $c_{0,\rm UT}^{\rm I}$ by $\sqrt{-t}/Q$ with respect to $c_{1,\rm UU}^{\rm I}$ and $c_{1,\rm UT}^{\rm I}$ is compensated by an enhancement from

y-dependent factors that are not shown, where $y = p \cdot q / p \cdot k$. These factors range from two to four in the kinematic conditions of the present measurement. The previously mentioned strong kinematic suppression of the squared DVCS amplitude relative to the interference term is partially compensated by the unshown kinematic factors that apply to Eqs. 6, 9 and 10. The net suppression is only about one order of magnitude in the HERMES kinematic conditions, and some sensitivity to the GPD E may therefore be provided by $c^{\mathrm{DVCS}}_{0,\mathrm{UT}}$. The coefficient $s^{\mathrm{I}}_{1,\mathrm{UT}}$ provides experimental sensitivity to the GPD $\widetilde{E}$, and also to $\widetilde{H}$, which was already probed experimentally through measurements of longitudinal target-spin asymmetries [17, 18]. The coefficients $c^{\mathrm{DVCS}}_{2,\mathrm{UT}}$, $s^{\mathrm{DVCS}}_{2,\mathrm{UT}}$, $c^{\mathrm{I}}_{3,\mathrm{UU}}$, $c^{\mathrm{I}}_{3,\mathrm{UT}}$ and $s^{\mathrm{I}}_{3,\mathrm{UT}}$ receive twist-two contributions involving the unknown gluon helicity-flip GPDs [19]. These GPDs do not mix with quark GPDs via Q^2 evolution and thus probe the intrinsic gluonic properties of the nucleon [20]. As the contribution of gluon helicity-flip is suppressed by the strong coupling constant α_S, this contribution competes with that from twist-four quark GPDs, which is suppressed by a factor M^2/Q^2 but not by α_s [21]. Aside from $c^{\mathrm{DVCS}}_{0,\mathrm{UU}}$ and $c^{\mathrm{DVCS}}_{2,\mathrm{UU}}$, all other coefficients appearing in Eqs. 4 and 5 are related to twist-three quark GPDs.

3. The experiment

Hard exclusive production of real photons in the reaction $ep^{\uparrow} \to e'\gamma p'$ is studied. Data with a transversely polarised hydrogen target [22] were accumulated using the HERMES spectrometer [23] and the longitudinally polarised 27.6 GeV electron and positron beams of the HERA accelerator at DESY. This final data set with the transversely polarised target was collected over the years 2002-2005. The integrated luminosities for the electron and positron samples are approximately 100 pb^{-1} and 70 pb^{-1}, respectively.

Events are selected if there were detected exactly one photon and one charged track identified as the scattered lepton. The hadron contamination in the lepton sample is kept below 1% by combining the information from a transition-radiation detector, a preshower scintillator detector, and an electromagnetic calorimeter. The kinematic requirements imposed are 1 GeV$^2 < Q^2 < 10$ GeV^2, $0.03 < x_B < 0.35$, and $\nu < 22$ GeV. The real photon is identified through the appearance of a 'neutral signal cluster', which is defined as an energy deposition larger than 5 GeV in the calorimeter with a signal larger than 1 MeV in the preshower detector, and the absence of a corresponding charged track in the back region of the spectrometer. The angular separation $\theta_{\gamma^*\gamma}$ between the virtual and real photons is required to be larger than 5 mrad. This value is determined mainly by the lepton momentum resolution. An upper bound of 45 mrad is imposed on this angle in order to improve the signal-to-background ratio [24].

The recoiling proton was not detected. Instead, an 'exclusive' sample of events is selected by requiring the squared missing mass $M_X^2 = (q + p - q')^2$ of the reaction $ep \to e'\gamma X$ to be close to the squared proton mass, where q' is the four-momentum of the real photon. The selection criterion was chosen by means of a Monte Carlo (MC) simulation of the distribution in M_X^2. The simulation is shown in comparison with

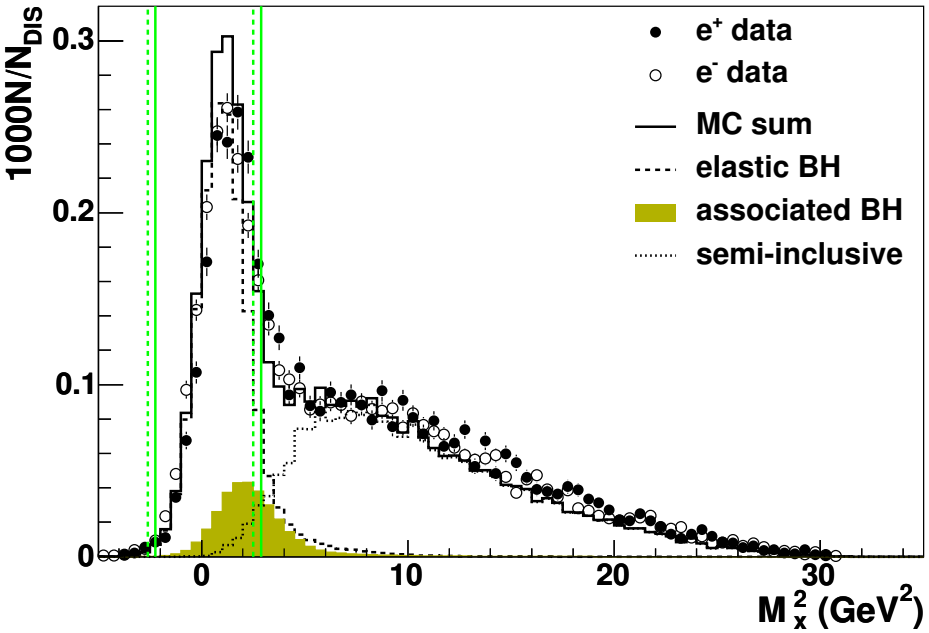

Figure 3. Distributions in squared missing-mass from data with positron (filled points) and electron (empty circles) beams and from Monte Carlo simulations (solid line). The latter include elastic BH (dashed line) and associated BH (filled area) processes as well as semi-inclusive background (dotted line). The simulations and data are both absolutely normalized. The vertical solid (dashed) lines enclose the selected exclusive region for the positron (electron) data. See text for details.

experimental data in Fig. 3. In the MC simulation [25], the Mo-Tsai formalism [26] is used for the elastic BH process that leaves the target nucleon intact, as well as the BH process where the nucleon is excited to a resonant state (a category known as associated production). For the latter, a parameterisation of the total $\gamma^* p$ cross section for the resonance region is used [27]. The individual cross sections for single-meson decay channels, e.g., $\Delta^+ \to p\pi^0$, are treated according to the MAID2000 model [28]. The remaining contribution is assigned to multi-meson decay channels, e.g., $\Delta^+ \to p\pi^0\pi^0$, whose relative contributions are determined according to isospin relations. The simulation also takes into account the semi-inclusive production of neutral mesons (mostly π^0) where either only one decay photon is detected or the decay photons cannot be resolved. For this, the MC generator LEPTO [29] is used in conjunction with a set of JETSET [30] fragmentation parameters that had previously been adjusted to reproduce multiplicity distributions observed by HERMES [31]. Not shown in Fig. 3 is the contribution from exclusive π^0 production, which is found to be less than 0.5% in the exclusive region using the model in Ref. [32]. The MC yield exceeds the data by about 20% in the exclusive region. This may be due to radiative effects not included in the simulation, which would move events from the peak to the continuum and improve the agreement [33]. On the other hand, if the DVCS process were included in the simulation, its contribution would increase the elastic peak. This contribution is highly

model-dependent and can vary between 10 and 25% [34]. The exclusive region for the positron data is chosen to be $-(1.5\ \mathrm{GeV})^2 < M_X^2 < (1.7\ \mathrm{GeV})^2$, where the value of $-(1.5\ \mathrm{GeV})^2$ is displaced from the squared proton mass by three times the resolution in M_X^2, and the value of $(1.7\ \mathrm{GeV})^2$ is the point where the contributions from the signal and background are equal. As the M_X^2 spectrum of the electron data is found to be shifted by approximately 0.18 GeV^2 towards smaller values relative to that of the positron data, the exclusive region for the electron data is shifted accordingly. One quarter of the effect of this shift on the results presented below is assigned as a systematic uncertainty contribution.

As the recoiling proton remains undetected, t is inferred from the measurement of the other final-state particles. For elastic events (leaving the proton intact), the kinematic relationship between the energy and direction of the real photon permits t to be calculated without using the measured energy of the real photon, which is the quantity subject to larger uncertainty. Thus the value of t in the exclusive region is calculated as

$$t = \frac{-Q^2 - 2\,\nu\,(\nu - \sqrt{\nu^2+Q^2}\,\cos\theta_{\gamma^*\gamma})}{1 + \frac{1}{M}\,(\nu - \sqrt{\nu^2+Q^2}\,cos\theta_{\gamma^*\gamma})}, \tag{12}$$

which is exact for elastic events. Using this method, the average resolution (RMS) in t is improved from 0.11 to 0.03 GeV^2. Exclusive events are selected with $-t < 0.7$ GeV^2 in order to reduce background.

4. Azimuthal asymmetries

Experimental observables that provide sensitivity to the coefficients appearing in Eqs. 4 and 5 are the Beam-Charge Asymmetry (BCA)

$$\mathcal{A}_{\mathrm{C}}(\phi) \equiv \frac{d\sigma^+(\phi) - d\sigma^-(\phi)}{d\sigma^+(\phi) + d\sigma^-(\phi)}, \tag{13}$$

and the Transverse Target-Spin Asymmetries (TTSAs)

$$\mathcal{A}_{\mathrm{UT}}^{\mathrm{DVCS}}(\phi,\phi_S) \equiv \frac{1}{S_\perp}\cdot\frac{d\sigma^+(\phi,\phi_S) - d\sigma^+(\phi,\phi_S+\pi) + d\sigma^-(\phi,\phi_S) - d\sigma^-(\phi,\phi_S+\pi)}{d\sigma^+(\phi,\phi_S) + d\sigma^+(\phi,\phi_S+\pi) + d\sigma^-(\phi,\phi_S) + d\sigma^-(\phi,\phi_S+\pi)}, \tag{14}$$

$$\mathcal{A}_{\mathrm{UT}}^{\mathrm{I}}(\phi,\phi_S) \equiv \frac{1}{S_\perp}\cdot\frac{d\sigma^+(\phi,\phi_S) - d\sigma^+(\phi,\phi_S+\pi) - d\sigma^-(\phi,\phi_S) + d\sigma^-(\phi,\phi_S+\pi)}{d\sigma^+(\phi,\phi_S) + d\sigma^+(\phi,\phi_S+\pi) + d\sigma^-(\phi,\phi_S) + d\sigma^-(\phi,\phi_S+\pi)}. \tag{15}$$

Here the subscripts on the $\mathcal{A}$'s represent dependence on beam Charge (C) or Transverse (T) target polarisation, with an Unpolarised (U) beam, and the superscripts $\pm$ stand for the lepton beam charge. These asymmetries are related to the coefficients in Eqs. 3–5

by:

$$\mathcal{A}_{\mathrm{C}}(\phi) = \frac{-\frac{K_{\mathrm{I}}}{\mathcal{P}_1(\phi)\mathcal{P}_2(\phi)}\sum_{n=0}^{3} c^{I}_{n,\mathrm{UU}}\cos(n\phi)}{\frac{K_{\mathrm{BH}}}{\mathcal{P}_1(\phi)\mathcal{P}_2(\phi)}\sum_{n=0}^{2} c^{\mathrm{BH}}_{n,\mathrm{UU}}\cos(n\phi) + K_{\mathrm{DVCS}}\sum_{n=0}^{2} c^{\mathrm{DVCS}}_{n,\mathrm{UU}}\cos(n\phi)} \tag{16}$$

$$\simeq \frac{-K_{\mathrm{I}}\left[c^{I}_{1,\mathrm{UU}}\cos(\phi)\right]}{K_{\mathrm{BH}}c^{\mathrm{BH}}_{0,\mathrm{UU}}}, \tag{17}$$

$$\mathcal{A}^{\mathrm{DVCS}}_{\mathrm{UT}}(\phi,\phi_S) = \frac{K_{\mathrm{DVCS}}\left[\sum_{n=0}^{2} c^{\mathrm{DVCS}}_{n,\mathrm{UT}}\sin(\phi-\phi_S)\cos(n\phi) + \sum_{n=1}^{2} s^{\mathrm{DVCS}}_{n,\mathrm{UT}}\cos(\phi-\phi_S)\sin(n\phi)\right]}{\frac{K_{\mathrm{BH}}}{\mathcal{P}_1(\phi)\mathcal{P}_2(\phi)}\sum_{n=0}^{2} c^{\mathrm{BH}}_{n,\mathrm{UU}}\cos(n\phi) + K_{\mathrm{DVCS}}\sum_{n=0}^{2} c^{\mathrm{DVCS}}_{n,\mathrm{UU}}\cos(n\phi)}, \tag{18}$$

$$\simeq \frac{K_{\mathrm{DVCS}}c^{\mathrm{DVCS}}_{0,\mathrm{UT}}\sin(\phi-\phi_S)}{\frac{K_{\mathrm{BH}}}{\mathcal{P}_1(\phi)\mathcal{P}_2(\phi)}c^{\mathrm{BH}}_{0,\mathrm{UU}}} \tag{19}$$

$$\mathcal{A}^{\mathrm{I}}_{\mathrm{UT}}(\phi,\phi_S) = \frac{-\frac{K_{\mathrm{I}}e_l}{\mathcal{P}_1(\phi)\mathcal{P}_2(\phi)}\left[\sum_{n=0}^{3} c^{\mathrm{I}}_{n,\mathrm{UT}}\sin(\phi-\phi_S)\cos(n\phi) + \sum_{n=1}^{3} s^{\mathrm{I}}_{n,\mathrm{UT}}\cos(\phi-\phi_S)\sin(n\phi)\right]}{\frac{K_{\mathrm{BH}}}{\mathcal{P}_1(\phi)\mathcal{P}_2(\phi)}\sum_{n=0}^{2} c^{\mathrm{BH}}_{n,\mathrm{UU}}\cos(n\phi) + K_{\mathrm{DVCS}}\sum_{n=0}^{2} c^{\mathrm{DVCS}}_{n,\mathrm{UU}}\cos(n\phi)} \tag{20}$$

$$\simeq \frac{-K_{\mathrm{I}}e_l\left[c^{\mathrm{I}}_{1,\mathrm{UT}}\sin(\phi-\phi_S)\cos\phi + s^{\mathrm{I}}_{1,\mathrm{UT}}\cos(\phi-\phi_S)\sin(\phi)\right]}{K_{\mathrm{BH}}c^{\mathrm{BH}}_{0,\mathrm{UU}}}. \tag{21}$$

HERMES reported the first measurement of the BCA [12], providing access to $c^{\mathrm{I}}_{1,\mathrm{UU}}$, the coefficient of the $\cos\phi$ modulation of the interference term for an unpolarised target. The present paper reports more precise BCA results using a considerably larger new data set from the first DVCS measurement done with transverse target polarisation. Most importantly, the extracted TTSAs provide access to $c^{\mathrm{DVCS}}_{0,\mathrm{UT}}$, $c^{\mathrm{I}}_{0,\mathrm{UT}}$ and $c^{\mathrm{I}}_{1,\mathrm{UT}}$, which are sensitive to the total angular momentum of quarks in the nucleon, as noted above.

4.1. Extraction of azimuthal asymmetry amplitudes

The distribution in the expectation value of the yield is given by:

$$\langle\mathcal{N}\rangle(S_\perp,e_l,\phi,\phi_S) = \mathcal{L}\,(S_\perp,e_l)\,\epsilon(e_l,\phi,\phi_S)\,\sigma_{UU}(\phi)\times \left[1 + S_\perp\mathcal{A}^{\mathrm{DVCS}}_{\mathrm{UT}}(\phi,\phi_S) + e_l\mathcal{A}_{\mathrm{C}}(\phi) + e_lS_\perp\mathcal{A}^{\mathrm{I}}_{\mathrm{UT}}(\phi,\phi_S)\right]. \tag{22}$$

Here $\mathcal{L}$ is the integrated luminosity, ϵ the detection efficiency, and σ_{UU} the cross section for an unpolarised target averaged over both beam charges. The BCA $\mathcal{A}_{\mathrm{C}}(\phi)$ and the TTSAs $\mathcal{A}^{\mathrm{DVCS}}_{\mathrm{UT}}(\phi,\phi_S)$ and $\mathcal{A}^{\mathrm{I}}_{\mathrm{UT}}(\phi,\phi_S)$ in Eq. 22 are expanded in terms of the same harmonics in ϕ and ϕ_S as those appearing in Eqs. 4 and 5 (as well as the harmonics $\cos(\phi-\phi_S)\sin(3\phi)$ and $\sin(\phi-\phi_S)\cos(3\phi)$ in Eq. 24, included as a systematic check):

$$\mathcal{A}_{\mathrm{C}}(\phi;\boldsymbol{\eta}_{\mathrm{C}}) = \sum_{n=0}^{3} A_{\mathrm{C}}^{\cos(n\phi)}\cos(n\phi), \tag{23}$$

$$\mathcal{A}^{\rm DVCS}_{\rm UT}(\phi,\phi_S;\boldsymbol{\eta}^{\rm DVCS}_{\rm UT}) = \sum_{n=0}^{3} A^{\sin(\phi-\phi_S)\cos(n\phi)}_{\rm UT,DVCS}\sin(\phi-\phi_S)\cos(n\phi) + \sum_{n=1}^{3} A^{\cos(\phi-\phi_S)\sin(n\phi)}_{\rm UT,DVCS}\cos(\phi-\phi_S)\sin(n\phi), \quad (24)$$

$$\mathcal{A}^{\rm I}_{\rm UT}(\phi,\phi_S;\boldsymbol{\eta}^{\rm I}_{\rm UT}) = \sum_{n=0}^{3} A^{\sin(\phi-\phi_S)\cos(n\phi)}_{\rm UT,I}\sin(\phi-\phi_S)\cos(n\phi) + \sum_{n=1}^{3} A^{\cos(\phi-\phi_S)\sin(n\phi)}_{\rm UT,I}\cos(\phi-\phi_S)\sin(n\phi). \quad (25)$$

Here $\boldsymbol{\eta}_{\rm C}$, $\boldsymbol{\eta}^{\rm DVCS}_{\rm UT}$ and $\boldsymbol{\eta}^{\rm I}_{\rm UT}$ represent the sets of Fourier coefficients or azimuthal asymmetry amplitudes, hereafter called 'asymmetry amplitudes', appearing in the right-hand sides of Eqs. 23–25 describing respectively the dependences of the squared DVCS amplitude and interference term on beam Charge (C), Transverse (T) target polarisation or both, with an Unpolarised (U) beam. These 18 asymmetry amplitudes embody the essential sensitivities to GPD models of the coefficients of the corresponding functions of ϕ appearing in Eqs. 4 and 5, to the degree that one can neglect the effects of the coefficients $c^{\rm BH}_{1,\rm UU}$ and $c^{\rm BH}_{2,\rm UU}$ and the squared unpolarised DVCS amplitude in Eqs. 18–20 and the effect of the ϕ-dependence of the BH propagators. In any case, the extracted asymmetry amplitudes are well defined and can be computed in various GPD models for direct comparison with the data. For each kinematic bin in $-t$, x_B or Q^2, they are simultaneously extracted from the observed exclusive event sample using the method of Maximum Likelihood. The distribution of events is parameterised by the function $\mathcal{N}_{\rm par}$, which is defined as

$$\mathcal{N}_{\rm par}(S_\perp,e_l,\phi,\phi_S;\boldsymbol{\eta}^{\rm DVCS}_{\rm UT},\boldsymbol{\eta}_{\rm C},\boldsymbol{\eta}^{\rm I}_{\rm UT}) = \mathcal{L}\,(S_\perp,e_l)\,\epsilon(e_l,\phi,\phi_S)\,\sigma_{UU}(\phi)\times \Big[1+S_\perp\mathcal{A}^{\rm DVCS}_{\rm UT}(\phi,\phi_S;\boldsymbol{\eta}^{\rm DVCS}_{\rm UT}) + e_l\mathcal{A}_{\rm C}(\phi;\boldsymbol{\eta}_{\rm C}) + e_l S_\perp\mathcal{A}^{\rm I}_{\rm UT}(\phi,\phi_S;\boldsymbol{\eta}^{\rm I}_{\rm UT})\Big]. \quad (26)$$

While the net beam polarisations of both positron and electron data samples used in the current measurement are not completely negligible (0.03 ± 0.02 and -0.03 ± 0.02, respectively), algebraic investigations (confirmed by MC studies) show that this does not affect the asymmetry amplitudes presented here. Not included in Eqs. 23-25 are negligible terms involving the small component of the target polarisation that is parallel to $\vec{q}$ [35].

Within the scheme known as Extended Maximum Likelihood [36], the likelihood function L to be minimized is taken as

$$-\ln L(\boldsymbol{\eta}^{\rm DVCS}_{\rm UT},\boldsymbol{\eta}_{\rm C},\boldsymbol{\eta}^{\rm I}_{\rm UT}) = \widetilde{\mathcal{N}}_{\rm par}(\boldsymbol{\eta}^{\rm DVCS}_{\rm UT},\boldsymbol{\eta}_{\rm C},\boldsymbol{\eta}^{\rm I}_{\rm UT}) - \sum_{i=1}^{N_{\rm o}}\ln\Big[1+S^i_\perp\mathcal{A}^{\rm DVCS}_{\rm UT}(\phi^i,\phi^i_S;\boldsymbol{\eta}^{\rm DVCS}_{\rm UT}) + e^i_l\mathcal{A}_{\rm C}(\phi^i;\boldsymbol{\eta}_{\rm C}) + e^i_l S^i_\perp\mathcal{A}^{\rm I}_{\rm UT}(\phi^i,\phi^i_S;\boldsymbol{\eta}^{\rm I}_{\rm UT})\Big], \quad (27)$$

where $N_{\rm o}$ is the observed number of events, and the parameterised total number $\widetilde{\mathcal{N}}_{\rm par}$ of events is

$$\widetilde{\mathcal{N}}_{\rm par}(\boldsymbol{\eta}_{\rm UT}^{\rm DVCS}, \boldsymbol{\eta}_{\rm C}, \boldsymbol{\eta}_{\rm UT}^{\rm I}) = \int {\rm d}S_\perp \, d\phi \, d\phi_S \sum_{e_l=\pm 1} \mathcal{N}_{\rm par}(S_\perp, e_l, \phi, \phi_S; \boldsymbol{\eta}_{\rm UT}^{\rm DVCS}, \boldsymbol{\eta}_{\rm C}, \boldsymbol{\eta}_{\rm UT}^{\rm I}). \quad (28)$$

The cross section σ_{UU} and the detection efficiency ϵ do not depend on $\boldsymbol{\eta}_{\rm UT}^{\rm DVCS}$, $\boldsymbol{\eta}_{\rm C}$ or $\boldsymbol{\eta}_{\rm UT}^{\rm I}$ and thus cannot affect the location of the likelihood maximum. Hence they have been omitted in the logarithms in Eq. 27. It is also not necessary to consider them explicitly in evaluating $\widetilde{\mathcal{N}}_{\rm par}(\boldsymbol{\eta}_{\rm UT}^{\rm DVCS}, \boldsymbol{\eta}_{\rm C}, \boldsymbol{\eta}_{\rm UT}^{\rm I})$ in Eq. 28, because the needed information about them is encoded in the total yields obtained by combining events for both target polarisations and beam charges. Luminosity imbalances between beam charges or target polarisations are taken into account by assigning weights w_i to the events, which are adjusted to provide effectively vanishing net target polarisation and net beam charge for this combined data set. The weights are normalized to also retain the same integrated luminosity $\mathcal{L}_{\,tot}$ as the observed 'unweighted' data sample. The resulting event distribution corresponds to the product $\mathcal{L}_{\,tot}\,\epsilon(\phi, \phi_S)\,\sigma_{UU}(\phi)$. In this manner, an event distribution corresponding to Eq. 26 is constructed to estimate the parameterised total number of events in Eq. 28:

$$\widetilde{\mathcal{N}}_{\rm par}(\boldsymbol{\eta}_{\rm UT}^{\rm DVCS}, \boldsymbol{\eta}_{\rm C}, \boldsymbol{\eta}_{\rm UT}^{\rm I}) \approx \sum_{i=1}^{N_{\rm o}} w_i \, \mathcal{L}\,(S_\perp, e_l)/\mathcal{L}_{\,tot} \times \Big[1 + S_\perp^i \mathcal{A}_{\rm UT}^{\rm DVCS}(\phi^i, \phi_S^i; \boldsymbol{\eta}_{\rm UT}^{\rm DVCS}) + e_l^i \mathcal{A}_{\rm C}(\phi^i; \boldsymbol{\eta}_{\rm C}) + e_l^i S_\perp^i \mathcal{A}_{\rm UT}^{\rm I}(\phi^i, \phi_S^i; \boldsymbol{\eta}_{\rm UT}^{\rm I})\Big].$$

4.2. Background corrections and systematic uncertainties

The results from the minimization of Eq. 27 in each kinematic bin are corrected for background from semi-inclusive and exclusive production of neutral mesons, mainly pions, in order to estimate the true asymmetry amplitude:

$$A_t = \frac{A_r - s \cdot A_s - e \cdot A_e}{1 - s - e}, \quad (29)$$

where A_r stands for the extracted raw asymmetry amplitude, and s and A_s (e and A_e) the fractional contribution and corresponding asymmetry amplitude of the semi-inclusive (exclusive) background. The combination of these background contributions $s + e$ ranges from $2 \pm 1\%$ to $11 \pm 5\%$ in the kinematic space [34]. As these background contributions are only very weakly beam-charge dependent, their asymmetries with respect to the beam charge or to the product of the beam charge and the transverse target polarisation are neglected. The asymmetry of the semi-inclusive π^0 background with respect to only the transverse target polarisation is extracted from experimental data by requiring two 'neutral signal clusters' in the calorimeter with their invariant mass between 0.10 and 0.17 GeV. The restriction on the energy deposition in the calorimeter

of the less energetic neutral signal cluster is relaxed to 1 GeV to improve the statistical precision. The fractional energy of the reconstructed neutral pions is required to be large, $z = E_\pi/\nu > 0.8$, as only these contribute to the exclusive region according to MC simulations [34]. These simulations showed that the extracted π^0 asymmetry does not depend on whether only one or both photons are in the acceptance. It is convenient to use the direction of the reconstructed pion in place of that of the photon to calculate the azimuthal angles ϕ and ϕ_S. For the exclusive π^0 background, the asymmetry amplitudes with respect to only target polarisation are not extracted due to the limited statistical precision but rather assumed to be 0 ± 1. After applying Eq. 29, the resulting asymmetry amplitude A_t is expected to originate from only elastic and associated production. On average 12% of the BH cross section arises from the latter [34], according to the simulation described above. The kinematic dependences of this contribution are shown in Fig. 4. No correction is made or uncertainty assigned for associated production, as it is considered to be part of the signal.

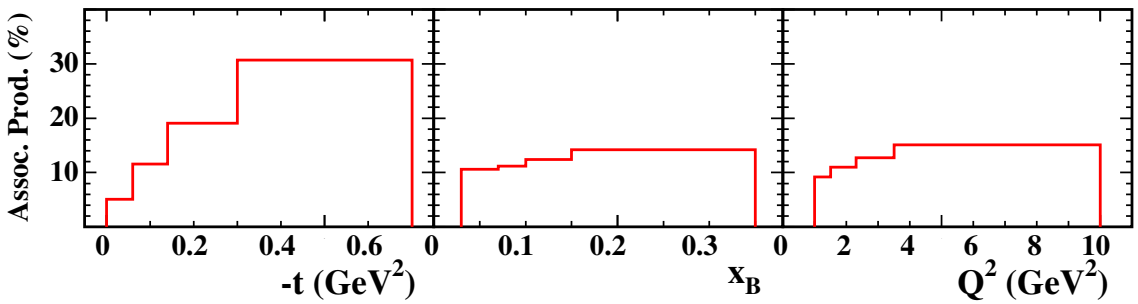

Figure 4. Kinematic dependences of the simulated fractional contributions from associated production. See text for details.

The dominant contributions to the total systematic uncertainty are those from the detector acceptance and finite bin width, and the determination of the target polarisation [34]. The combined contribution to the systematic uncertainty from the detector acceptance, finite bin width, and the alignment of the detector elements with respect to the beam, including possible effects from the beam and track curvature in the transverse magnetic field of the target, is determined from MC simulations based on five GPD models described in Ref. [37]. In each kinematic bin, it is defined as the RMS difference between the asymmetry amplitude extracted from the MC data in that bin by minimizing Eq. 27 and the corresponding model predictions calculated analytically at the mean kinematic values of that bin given in Table 1. The other sources are associated with the background correction, calorimeter calibration and the relative shift of the M_X^2 spectra between the positron and electron data. These contributions, given in Table 2, are added in quadrature to form the total systematic uncertainty per kinematic bin, appearing in Table 1. Not included is any contribution due to additional QED vertices, as the most significant of these has been estimated to be negligible [38].

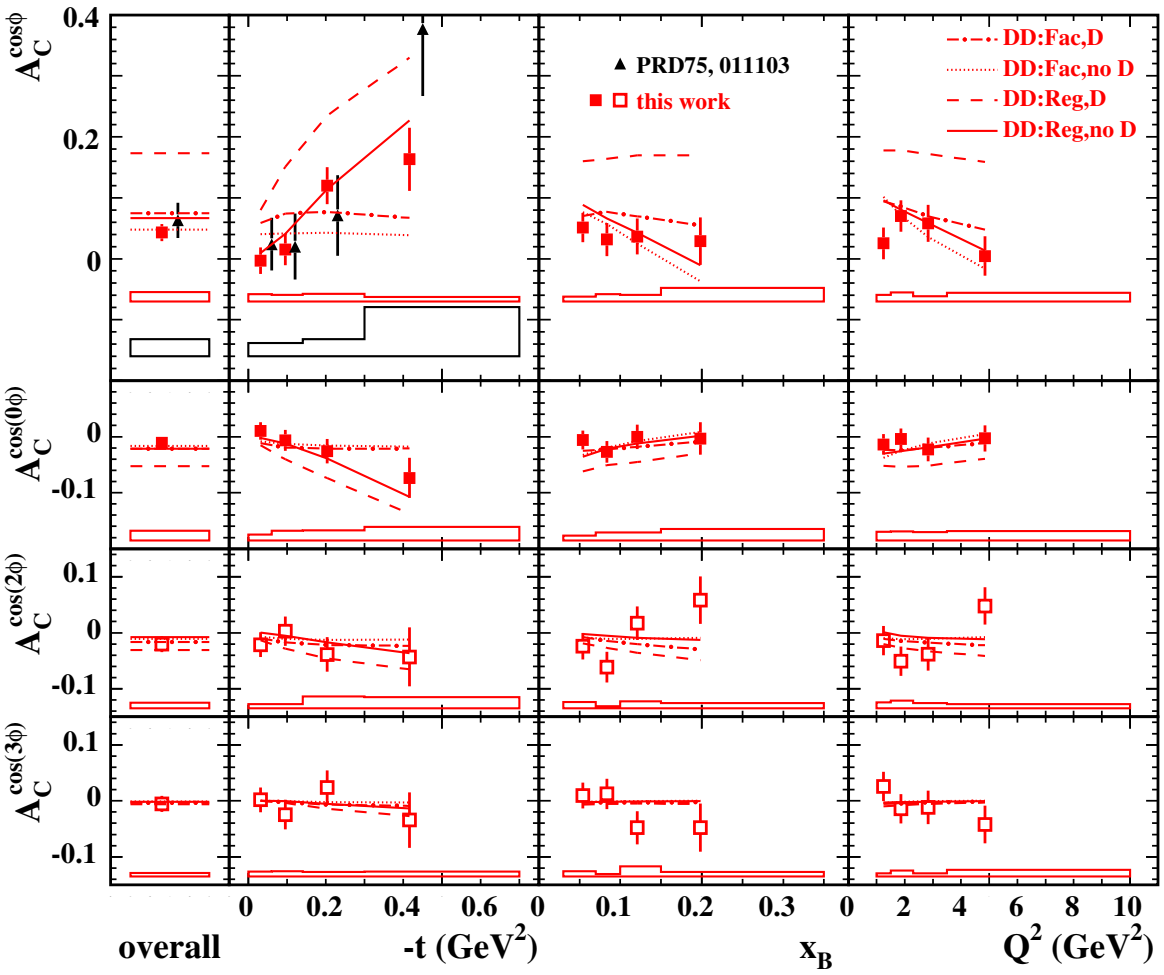

Figure 5. Asymmetry amplitudes describing the dependence of the interference term on the beam charge (A_C), for the exclusive sample. The squares represent the results from the present work, while data represented by triangles (shifted right for visibility) were reported in Ref. [12]. The filled symbols indicate those results of greatest interest (see text). The error bars (bands) represent the statistical (systematic) uncertainties. The curves are predictions of variants of a double-distribution GPD model [32, 39], with profile parameters given in Table 3. See text for details.

5. Results

Figures 5–7 show as a function of $-t$, x_B or Q^2, in four bins, the results from the combined fit. The 'overall' results in the left-most columns correspond to the entire experimental acceptance. Fig. 5 shows the amplitudes related to only beam charge, while Figs. 6 and 7 show the amplitude $A_{\mathrm{UT,DVCS}}$, which relates to transverse target polarisation only, and $A_{\mathrm{UT,I}}$, which relates to both. For simplicity of presentation, the amplitudes $A_{\mathrm{UT,DVCS}}$ and $A_{\mathrm{UT,I}}$ for the same azimuthal dependence are shown together in each panel, even though they typically do not relate to the same GPDs. The filled symbols represent the asymmetry amplitudes of interest here (see Table 1), related to

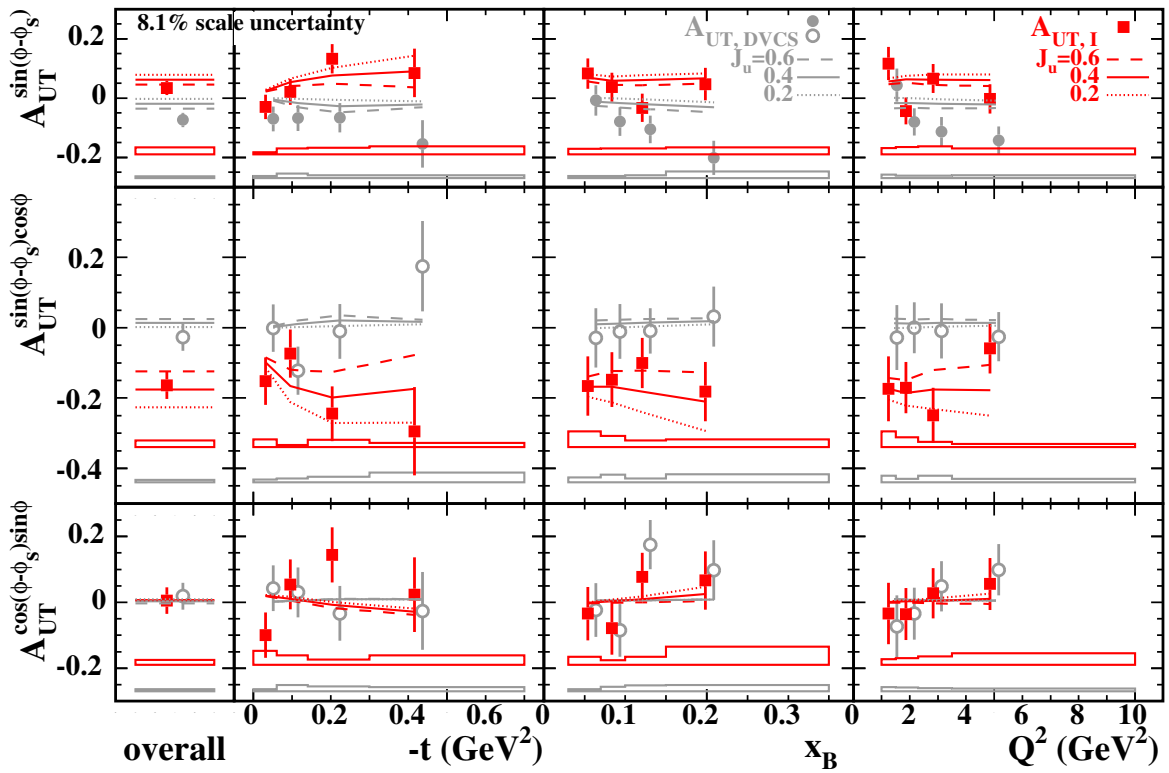

Figure 6. Asymmetry amplitudes describing the dependence of the squared DVCS amplitude (circles, $A_{\mathrm{UT,DVCS}}$) and the interference term (squares, $A_{\mathrm{UT,I}}$) on the transverse target polarisation, for the exclusive sample. The filled symbols indicate those results of greatest interest (see text). The circles (squares) are shifted right (left) for visibility. The error bars represent the statistical uncertainties, while the top (bottom) bands denote the systematic uncertainties for $A_{\mathrm{UT,I}}$ ($A_{\mathrm{UT,DVCS}}$), excluding the 8.1 % scale uncertainty from the target polarisation measurement. The curves are predictions of the GPD model variant (Reg, no D) shown in Fig. 5 as a continuous curve, with three different values for the u-quark total angular momentum J_u and fixed d-quark total angular momentum $J_d = 0$ [16]. See text for details.

the coefficients given in Eqs. 6–11, of the corresponding harmonics of ϕ appearing in Eqs. 4 and 5.

Of particular interest is the asymmetry amplitude $A_{\mathrm{C}}^{\cos\phi}$ in the upper row of Fig. 5. Equation 7 shows that this amplitude is sensitive to the GPD H in the HERMES kinematic conditions. Also shown in this figure is the previously published result, which has been shown to constrain GPD models [12]. The greatly improved precision of the present measurement confirms that this amplitude increases with increasing $-t$. As mentioned above regarding the corresponding coefficients $c^{\mathrm{I}}_{0,\mathrm{UU}}$ and $c^{\mathrm{I}}_{1,\mathrm{UU}}$, the amplitude $A_{\mathrm{C}}^{\cos 0\phi}$ is expected to relate to the same combination of GPDs as does $A_{\mathrm{C}}^{\cos\phi}$. The results shown in Fig. 5 suggest that the magnitude of this amplitude also increases with $-t$, while its opposite sign is expected from Eq. 8.

Of special interest in this work are the amplitudes $A_{\mathrm{UT,I}}^{\sin(\phi-\phi_S)\cos(n\phi)}, n = 0, 1$, presented in the top two rows of Fig. 6. Equations 10 and 9 show that these amplitudes

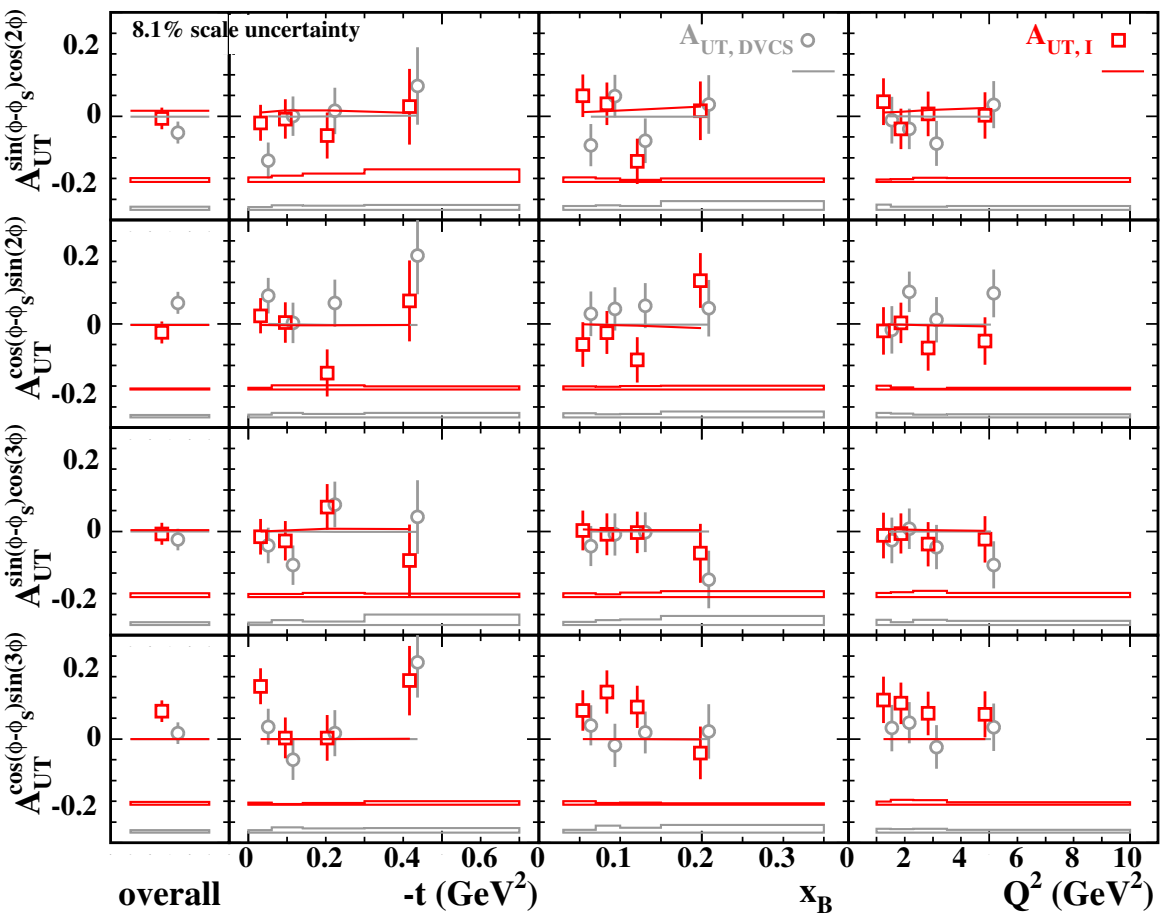

Figure 7. Asymmetry amplitudes that are expected to be suppressed, presented as in Fig. 6, except that the curves are calculated only for $J_u = 0.4$.

are sensitive to the GPD E and hence to the total angular momenta of quarks. These amplitudes are found to have substantial magnitudes with opposite signs but little kinematic dependence, possibly increasing in magnitude with $-t$. Their opposite signs are expected from Eq. 10. Also of interest is the amplitude $A_{\mathrm{UT,DVCS}}^{\sin(\phi-\phi_S)}$, shown in the top row of Fig. 6, which Eq. 6 suggests is also sensitive to the GPD E. The overall result is non-zero by 2.8 times the total uncertainty. These data tend to increase in magnitude at larger values of Q^2. (In fixed-target experiments, x_B and Q^2 are strongly correlated.) They provide the first experimental evidence for an azimuthal harmonic in the squared DVCS amplitude, in this case related to transverse target polarisation.

The amplitude $A_{UT,I}^{\cos(\phi-\phi_S)\sin\phi}$ shown in the bottom row of Fig. 6 is sensitive mainly to the GPDs $\widetilde{H}$ and $\widetilde{E}$, while the contribution from the GPD E is suppressed by an additional factor of x_B (see Eq. 11). The measured asymmetry amplitudes are consistent with zero.

The amplitudes represented by the unfilled symbols are expected to be suppressed, and are indeed found to be typically small. However, values that depart from zero by

more than twice the total uncertainty are found for the entire experimental acceptance for two of the four amplitudes in Fig. 7 that receive a contribution from gluon helicity-flip, which are $A_{\mathrm{UT,DVCS}}^{\cos(\phi-\phi_S)\sin(2\phi)}$ and $A_{\mathrm{UT,I}}^{\cos(\phi-\phi_S)\sin(3\phi)}$. The asymmetry amplitudes related to the squared DVCS amplitude in the bottom two rows of Fig. 7 correspond to coefficients that do not appear in Eq. 4 as a consequence of the one-photon exchange approximation. They are found to be consistent with zero.

6. Comparison with theory

The data are compared with various theoretical calculations to LO in α_{em} and α_s, which do not account for the contributions of associated production. The calculations shown in Figs. 5–7 employ variants of a GPD model developed in Refs. [32, 39]. These are based on the widely used framework of double distributions involving a product of PDFs representing the forward limit and a profile function representing the skewness dependence [40]. The forward limits of the GPDs H_q are constructed using the MRST98 [41] parameterisation of PDFs evaluated at the measured Q^2 value for each data point. More modern parameterisations are expected to result in a negligible difference [16]. In the model description for $\widetilde{H}$ and $\widetilde{E}$, the forward limit of the GPD $\widetilde{H}$ is fixed by the quark helicity distributions $\Delta q(x_B, Q^2)$, while the GPD $\widetilde{E}$ is evaluated from the pion pole, which provides only the real part. The 'profile parameters' b_{val} and b_{sea} control the skewness dependence of GPDs for the valence and sea quarks, respectively [40, 42]. The t dependence of the GPDs is calculated in either the simplest ansatz where the t dependence factorises from the t–independent part $H_q(x,\xi)$, or in the Regge-inspired ansatz. The GPDs H and E are optionally modified by the so-called (t–independent) D–term [43] contribution to the double-distribution part of the GPD, with a value calculated in the chiral–quark soliton model [44]. The twist-three GPDs are treated in the Wandzura-Wilczek approximation, and the gluon helicity-flip GPDs are not included. The quark total angular momenta J_q of quarks and antiquarks of flavour q (q = u,d) enter as model parameters for the GPD E. The strange sea is neglected. The computational program of Ref. [45] is used. The calculation is done at the average kinematics of every bin (see Table 1). For the comparison of the BCA amplitudes to the double-distribution model shown in Fig. 5, the model variations of interest are those that change the GPD H, since the impact of the GPDs $\widetilde{H}$ and E is suppressed at HERMES kinematic conditions (see Eq. 7). Four different variants are selected by choosing either a factorised (Fac) or a Regge-inspired (Reg) t dependence, each with or without the contribution of the D-term. While these four variants lead to very different model predictions for $A_{\mathrm{C}}^{\cos\phi}$ as illustrated in the figure, the variation of the profile parameters b_{val} and b_{sea} lead to smaller changes [24]. However, by comparing the data for the $\cos\phi$ amplitude with predictions of all four variants of this model in combination with four specific sets of values for the profile parameters, it is found that the calculation using the Regge-inspired t dependence without the D–term and $b_{val} = \infty$, $b_{sea} = 1$ results in a confidence level much higher than all the alternatives. Here, $b = 1$

corresponds to a substantial skewness dependence, which is eliminated for $b = \infty$. All the variants shown in Fig. 5 are calculated using profile parameter values that yield the best agreement with data (see Table 3). For any choice of the profile parameters, the variant Regge with a D-term is excluded, while the factorised ansatz is disfavoured either with or without the D-term. The factorised t dependence is also disfavoured on theoretical grounds [46, 47].

The theoretical calculations of the TTSA amplitudes shown in Figs. 6 and 7 are made using the Regge inspired t dependence without the D-term and $b_{val} = \infty$ and $b_{sea} = 1$, a combination that is favoured by the BCA data as described above. However, while the calculated TTSA amplitudes are less sensitive to that choice, some of them are quite sensitive to the choice of the quark total angular momenta J_q [16]. This sensitivity is illustrated by the curves in Fig. 6 evaluated with three different values of J_u (0.2, 0.4, 0.6), while fixing $J_d = 0$ [16]. Although this model fails to describe the data for $A_{UT,\mathrm{DVCS}}^{\sin(\phi-\phi_S)}$, the model curves confirm the expectation from Eqs. 6, 9 and 10 that the TTSA amplitudes $A_{UT,\mathrm{DVCS}}^{\sin(\phi-\phi_S)}$, $A_{UT,\mathrm{I}}^{\sin(\phi-\phi_S)\cos\phi}$ and $A_{UT,\mathrm{I}}^{\sin(\phi-\phi_S)}$ have significant sensitivity to J_u. However, for this double-distribution model, the amplitudes related to the interference term are in reasonable agreement with the data, of which $A_{UT,\mathrm{I}}^{\sin(\phi-\phi_S)\cos\phi}$ has the greatest sensitivity. The curves in Fig. 5 and 7 are evaluated with fixed $J_u = 0.4$ and $J_d = 0$, since the sensitivity here to J_u and J_d is negligible.

The BCA amplitude $A_{\mathrm{C}}^{\cos\phi}$ and the TTSA amplitudes $A_{UT,\mathrm{I}}^{\sin(\phi-\phi_S)}$ and $A_{UT,\mathrm{I}}^{\sin(\phi-\phi_S)\cos\phi}$ are also compared to calculations based on the 'dual-parameterisation' model of GPDs [48, 49] in Figs. 8 and 9. Calculations for all other amplitudes are not shown since the model contains neither GPDs $\widetilde{H}$ and $\widetilde{E}$ nor higher-twist contributions. For the BCA amplitude, the curves in Fig. 8 are evaluated with fixed $J_u = J_d = 0$, which best describes the TTSA amplitudes as discussed below. The t dependence of the GPDs is assumed to be either factorised and exponential, or non-factorised and Regge-inspired [39]. Both choices describe the BCA data equally well, but with a smaller confidence level (χ^2/d.o.f.=2.2 for both Fac and Reg) than the favoured double-distribution model described above. On the other hand, the existing beam-spin asymmetry data [51] are better described by this dual-parameterisation model. The Regge-inspired variant of this model with $J_u = 0$, 0.2, and 0.4, and $J_d = 0$ is used for the calculations shown in Fig. 9. It is apparent that also in the dual-parameterisation model, the amplitudes $A_{UT,\mathrm{I}}^{\sin(\phi-\phi_S)\cos\phi}$ and $A_{UT,\mathrm{I}}^{\sin(\phi-\phi_S)}$ are sensitive to J_u.

7. Quark total angular momentum

In either GPD model discussed above, the GPD E is parameterised in terms of J_u and J_d [39, 16]. In both cases these two parameters are fit to the measured overall TTSA amplitudes $A_{\mathrm{UT,I}}^{\sin(\phi-\phi_S)\cos\phi}$ and $A_{\mathrm{UT,I}}^{\sin(\phi-\phi_S)}$ appearing in the left column of Figs. 6 and 9, respectively. The other parameters for the respective GPD models are the same as used for the curves in Figs. 6 or 9. The area in the (J_u, J_d)-plane in which the reduced $\chi^2 - \chi^2_{min}$ value is not larger than unity corresponds to a one-standard-deviation

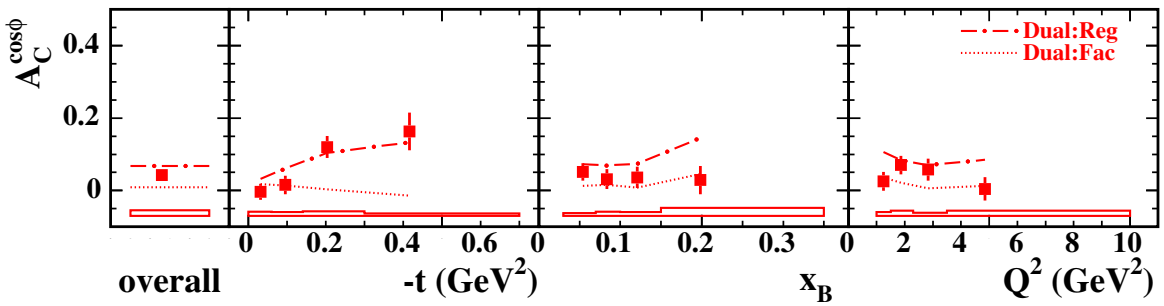

Figure 8. Similar to the top row of Fig. 5, except that the curves are calculations [50] based on the dual-parameterisation GPD model [49]. See text for details.

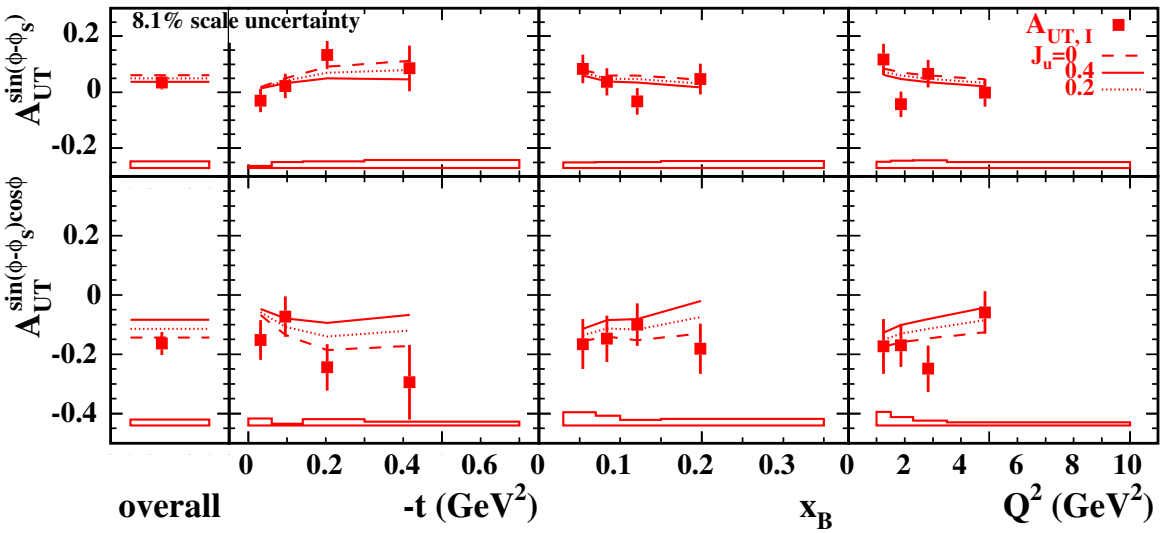

Figure 9. Similar to top two rows of Fig. 6, except that the curves are the calculations [50] using the Regge-inspired form of the t dependence in the dual-parameterisation GPD model [49] (shown in Fig. 8 as a dash-dotted curve), with three different values for the u-quark total angular momentum J_u and fixed d-quark total angular momentum $J_d = 0$. See text for details.

constraint on J_u vs J_d. This area is found to be one of the sloped bands in Fig. 10, which in units of $\hbar$ can be represented in the case of the double-distribution model as

$$J_u + J_d/2.8 = 0.49 \pm 0.17(\exp_{\rm tot}), \tag{30}$$

and in the case of the dual-parameterisation model as

$$J_u + J_d/2.8 = -0.02 \pm 0.27(\exp_{\rm tot}). \tag{31}$$

The uncertainty is propagated from the total experimental uncertainty in the measured TTSA amplitudes. This uncertainty dominates the effects of variations within either of the GPD models of the values of profile parameters b and the inclusion of the D term. The variation of the value of $J_u + J_d/2.8$ obtained by fitting the amplitudes in the bins of the three kinematic variables is found to be not larger than ± 0.15. The

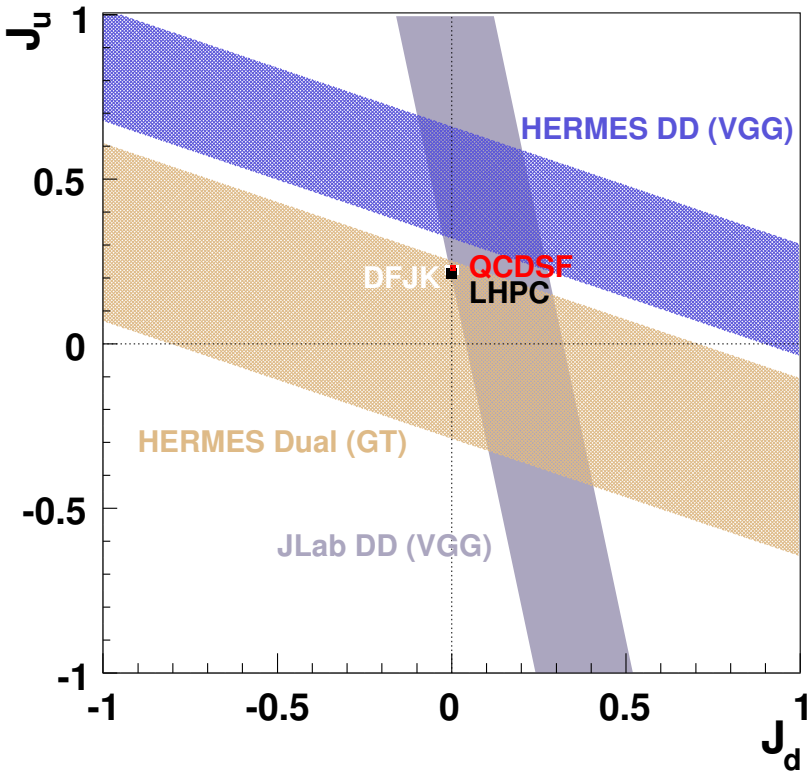

Figure 10. Model-dependent constraints on u-quark total angular momentum J_u vs d-quark total angular momentum J_d, obtained by comparing DVCS experimental results and theoretical calculations. The constraints based on the HERMES data for the TTSA amplitudes $A_{\mathrm{UT}}^{\sin(\phi-\phi_S)\cos\phi}$ and $A_{\mathrm{UT,I}}^{\sin(\phi-\phi_S)}$ use the double-distribution (HERMES DD) [32, 39] or dual-parameterisation (HERMES Dual) [49] GPD models. The additional band (JLab DD) is derived from the comparison of the double-distribution GPD model with neutron cross section data [55]. Also shown as small (overlapping) rectangles are results from lattice gauge theory by the QCDSF [52] and LHPC [47] collaborations, as well as a result for only the valence quark contribution (DFJK) based on zero-skewness GPDs extracted from nucleon form factor data [53, 54]. The sizes of the small rectangles represent the statistical uncertainties of the lattice gauge results, and the parameter range for which a good DFJK fit to the nucleon form factor data was achieved. Theoretical uncertainties are unavailable.

results from fitting the two azimuthal amplitudes separately were found to be consistent. The large difference between the constraints obtained using the double-distribution and dual-parameterisation models is an indication of a large model dependence of the (J_u, J_d) constraint obtained, which may be related to the failure of both models to fully describe all other available DVCS data. Both constraints are consistent with results, also shown in Fig. 10, from unquenched lattice gauge simulations by the QCDSF [52] and the LHPC [47] collaborations. The statistical uncertainties of the lattice gauge results are comparable to the size of the plotted symbols. The QCDSF calculation of the first moments of the GPDs, the so-called generalized form factors, is based on a simulation using dynamical Wilson fermions with pion masses down to 350 MeV. The dynamical LHPC calculation is based on a hybrid approach of rooted staggered sea and

domain wall valence quarks. In both calculations the generalized form factors have been simultaneously extrapolated in t and m_π^2 to $t = 0$ and the physical point, respectively, using the same results from chiral perturbation theory. Both calculations include only contributions from connected diagrams. The uncertainties are primarily statistical but include some systematic uncertainties from the chiral, continuum and infinite volume extrapolations. Also shown in Fig. 10 is a result for only the valence contribution to the quark total angular momenta [53, 54]. It is based on the extraction of zero-skewness GPDs from nucleon form factor data, assuming handbag diagram dominance and exploiting well known sum rules. The size of the plotted symbol corresponds to the parameter range for which a good fit to the nucleon form factor data was achieved.

Table 1. Results of particular interest for the asymmetry amplitudes of the asymmetries with respect to the beam charge and transverse target polarisation for the exclusive sample.

kinematic bin		$\langle -t \rangle$ (GeV^2)	$\langle x_B \rangle$	$\langle Q^2 \rangle$ (GeV^2)	$A_{\mathrm{C}}^{\cos(0\phi)}$ $\pm\delta_{\mathrm{stat}} \pm \delta_{\mathrm{syst}}$	$A_{\mathrm{C}}^{\cos\phi}$ $\pm\delta_{\mathrm{stat}} \pm \delta_{\mathrm{syst}}$	$A_{\mathrm{UT,DVCS}}^{\sin(\phi-\phi_S)}$ $\pm\delta_{\mathrm{stat}} \pm \delta_{\mathrm{syst}}$
overall		0.12	0.09	2.5	$-0.011 \pm 0.010 \pm 0.017$	$0.043 \pm 0.014 \pm 0.015$	$-0.073 \pm 0.024 \pm 0.008$
$-t$(GeV^2)	0.00–0.06	0.03	0.08	1.9	$0.010 \pm 0.016 \pm 0.010$	$-0.003 \pm 0.022 \pm 0.012$	$-0.070 \pm 0.041 \pm 0.009$
	0.06–0.14	0.10	0.10	2.5	$-0.006 \pm 0.019 \pm 0.017$	$0.015 \pm 0.026 \pm 0.011$	$-0.067 \pm 0.043 \pm 0.017$
	0.14–0.30	0.20	0.11	2.9	$-0.026 \pm 0.022 \pm 0.018$	$0.120 \pm 0.030 \pm 0.012$	$-0.066 \pm 0.050 \pm 0.011$
	0.30–0.70	0.42	0.12	3.5	$-0.074 \pm 0.036 \pm 0.024$	$0.163 \pm 0.052 \pm 0.007$	$-0.153 \pm 0.080 \pm 0.015$
x_B	0.03–0.07	0.10	0.05	1.5	$-0.006 \pm 0.017 \pm 0.009$	$0.051 \pm 0.024 \pm 0.008$	$-0.008 \pm 0.051 \pm 0.008$
	0.07–0.10	0.10	0.08	2.2	$-0.027 \pm 0.019 \pm 0.014$	$0.032 \pm 0.027 \pm 0.012$	$-0.079 \pm 0.049 \pm 0.010$
	0.10–0.15	0.13	0.12	3.1	$0.000 \pm 0.022 \pm 0.014$	$0.037 \pm 0.030 \pm 0.011$	$-0.105 \pm 0.047 \pm 0.013$
	0.15–0.35	0.20	0.20	5.0	$-0.003 \pm 0.029 \pm 0.021$	$0.029 \pm 0.039 \pm 0.022$	$-0.201 \pm 0.058 \pm 0.027$
Q^2(GeV^2)	1.0–1.5	0.08	0.06	1.2	$-0.014 \pm 0.019 \pm 0.016$	$0.025 \pm 0.026 \pm 0.011$	$0.044 \pm 0.056 \pm 0.012$
	1.5–2.3	0.10	0.08	1.9	$-0.004 \pm 0.018 \pm 0.016$	$0.070 \pm 0.026 \pm 0.015$	$-0.080 \pm 0.046 \pm 0.010$
	2.3–3.5	0.13	0.11	2.8	$-0.023 \pm 0.021 \pm 0.015$	$0.058 \pm 0.030 \pm 0.008$	$-0.113 \pm 0.049 \pm 0.012$
	3.5–10.0	0.19	0.17	4.9	$-0.003 \pm 0.023 \pm 0.016$	$0.005 \pm 0.032 \pm 0.014$	$-0.143 \pm 0.048 \pm 0.015$

kinematic bin		$\langle -t \rangle$ (GeV^2)	$\langle x_B \rangle$	$\langle Q^2 \rangle$ (GeV^2)	$A_{\mathrm{UT,I}}^{\sin(\phi-\phi_S)}$ $\pm\delta_{\mathrm{stat}} \pm \delta_{\mathrm{syst}}$	$A_{\mathrm{UT,I}}^{\sin(\phi-\phi_S)\cos\phi}$ $\pm\delta_{\mathrm{stat}} \pm \delta_{\mathrm{syst}}$	$A_{\mathrm{UT,I}}^{\cos(\phi-\phi_S)\sin\phi}$ $\pm\delta_{\mathrm{stat}} \pm \delta_{\mathrm{syst}}$
overall		0.12	0.09	2.5	$0.035 \pm 0.024 \pm 0.024$	$-0.164 \pm 0.039 \pm 0.023$	$0.005 \pm 0.040 \pm 0.015$
$-t$(GeV^2)	0.00–0.06	0.03	0.08	1.9	$-0.030 \pm 0.031 \pm 0.008$	$-0.152 \pm 0.068 \pm 0.026$	$-0.100 \pm 0.069 \pm 0.044$
	0.06–0.14	0.10	0.10	2.5	$0.022 \pm 0.044 \pm 0.021$	$-0.073 \pm 0.068 \pm 0.008$	$0.054 \pm 0.076 \pm 0.030$
	0.14–0.30	0.20	0.11	2.9	$0.133 \pm 0.050 \pm 0.025$	$-0.244 \pm 0.078 \pm 0.028$	$0.144 \pm 0.083 \pm 0.020$
	0.30–0.70	0.42	0.12	3.5	$0.085 \pm 0.082 \pm 0.028$	$-0.294 \pm 0.126 \pm 0.026$	$0.024 \pm 0.113 \pm 0.029$
x_B	0.03–0.07	0.10	0.05	1.5	$0.083 \pm 0.051 \pm 0.021$	$-0.166 \pm 0.084 \pm 0.047$	$-0.034 \pm 0.081 \pm 0.025$
	0.07–0.10	0.10	0.08	2.2	$0.037 \pm 0.048 \pm 0.021$	$-0.148 \pm 0.078 \pm 0.034$	$-0.078 \pm 0.080 \pm 0.015$
	0.10–0.15	0.13	0.12	3.1	$-0.033 \pm 0.048 \pm 0.021$	$-0.100 \pm 0.072 \pm 0.020$	$0.078 \pm 0.073 \pm 0.025$
	0.15–0.35	0.20	0.20	5.0	$0.048 \pm 0.055 \pm 0.024$	$-0.182 \pm 0.084 \pm 0.026$	$0.066 \pm 0.088 \pm 0.056$
Q^2(GeV^2)	1.0–1.5	0.08	0.06	1.2	$0.117 \pm 0.056 \pm 0.024$	$-0.174 \pm 0.092 \pm 0.047$	$-0.034 \pm 0.093 \pm 0.018$
	1.5–2.3	0.10	0.08	1.9	$-0.043 \pm 0.046 \pm 0.026$	$-0.170 \pm 0.073 \pm 0.031$	$-0.036 \pm 0.079 \pm 0.020$
	2.3–3.5	0.13	0.11	2.8	$0.066 \pm 0.049 \pm 0.028$	$-0.249 \pm 0.078 \pm 0.025$	$0.028 \pm 0.076 \pm 0.026$
	3.5–10.0	0.19	0.17	4.9	$-0.002 \pm 0.049 \pm 0.020$	$-0.059 \pm 0.072 \pm 0.011$	$0.056 \pm 0.079 \pm 0.035$

8. Conclusions

Transverse target-spin azimuthal asymmetries in electroproduction of real photons are measured for the first time, and for both beam charges. A combined fit of this data set separates for the first time the azimuthal harmonics of the squared DVCS amplitude and the interference term. The extracted charge asymmetry of the interference term is much more precise than previously published results, and constrains models for Generalized Parton Distributions. By comparing GPD-model calculations with extracted azimuthal asymmetry amplitudes associated with both beam charge and transverse-target polarisation, a model-dependent constraint on the total angular momenta carried by u and d-quarks in the nucleon is obtained as $J_u + J_d/2.8 = 0.49 \pm 0.17(\exp_{\rm tot})$ using a double-distribution GPD model, and $J_u + J_d/2.8 = -0.02 \pm 0.27(\exp_{\rm tot})$ using the dual-parameterisation model. Thus, such data have the potential to provide quantitative information about the spin content of the nucleon when GPD models become available that fully describe all existing DVCS data.

Table 2. Systematic uncertainties of the results of particular interest for the azimuthal amplitudes of the asymmetries with respect to the beam charge and transverse target polarisation for the exclusive sample. Those results involving transverse target polarisation are also subject to an additional 8.1% scale uncertainty from the determination of the target polarisation.

Source	$A_{\rm C}^{\cos(0\phi)}$	$A_{\rm C}^{\cos\phi}$	$A_{\rm UT,\,DVCS}^{\sin(\phi-\phi_S)}$	$A_{\rm UT,\,I}^{\sin(\phi-\phi_S)}$	$A_{\rm UT,\,I}^{\sin(\phi-\phi_S)\cos\phi}$	$A_{\rm UT,\,I}^{\cos(\phi-\phi_S)\sin\phi}$
M_X^2 shift	0.004	0.001	0.000	0.000	0.001	0.001
Background correction	0.000	0.001	0.005	0.001	0.004	0.000
Calorimeter calibration	0.001	0.003	0.002	0.002	0.005	0.003
Acceptance, bin width, alignment	0.017	0.015	0.002	0.024	0.019	0.014

Acknowledgments

We gratefully acknowledge the DESY management for its support and the staff at DESY and the collaborating institutions for their significant effort. We are also grateful for careful reading and advice by Markus Diehl and Dieter Müller. This work was supported by the FWO-Flanders, Belgium; the Natural Sciences and Engineering Research Council of Canada; the National Natural Science Foundation of China; the Alexander von Humboldt Stiftung; the German Bundesministerium für Bildung und Forschung (BMBF); the Deutsche Forschungsgemeinschaft (DFG); the Italian Istituto Nazionale di Fisica Nucleare (INFN); the MEXT, JSPS, and COE21 of Japan; the Dutch

Table 3. The quality of agreement between the measured $A_C^{\cos(\phi)}$ asymmetry amplitude and four variants of the double-distribution model. These χ^2 values are based on sums over the 12 bins in $-t$, x_B and Q^2, without considering the correlations among them because of their sharing of some events. The values given are the sums divided by 12. Values shown in bold face denote for each variant the profile parameter set that yields the best agreement with the data, chosen to produce the curves in Fig. 5.

χ^2/d.o.f. ($J_u = 0.4$)	$b_v = b_s = 1$	$b_v = 1$, $b_s = \infty$	$b_v = \infty$, $b_s = 1$	$b_v = b_s = \infty$
Fac, D	4.2	16.0	**2.3**	10.5
Fac, no D	4.5	**2.3**	7.9	3.3
Reg, D	22.2	37.4	**16.5**	29.2
Reg, no D	2.5	7.0	**1.1**	3.8

Foundation for Fundamenteel Onderzoek der Materie (FOM); the U. K. Engineering and Physical Sciences Research Council, the Particle Physics and Astronomy Research Council and the Scottish Universities Physics Alliance; the U. S. Department of Energy (DOE) and the National Science Foundation (NSF) and the Ministry of Trade and Economical Development and the Ministry of Education and Science of Armenia.

References

[1] D. Müller *et al.*, Fortschr. Phys. **42** (1994) 101.
[2] X. Ji, Phys. Rev. Lett. **78** (1997) 610; Phys. Rev. **D55** (1997) 7114.
[3] A.V. Radyushkin, Phys. Rev. **D56** (1997) 5524.
[4] M. Burkardt, Phys. Rev. **D62** (2000) 071503; Erratum–ibid. **D66** (2002) 119903.
[5] M. Diehl, Eur. Phys. J. **C25** (2002) 223; Erratum-ibid. **C31** (2003) 277.
[6] J.P. Ralston and B. Pire, Phys. Rev. **D66** (2002) 111501.
[7] A.V. Belitsky and D. Müller, Nucl. Phys. **A711** (2002) 118.
[8] M. Burkardt, Int. J. Mod. Phys. **A18** (2003) 173.
[9] HERMES Collaboration, A. Airapetian *et al.*, Phys. Rev. Lett. **87** (2001) 182001.
[10] CLAS Collaboration, S. Stepanyan *et al.*, Phys. Rev. Lett. **87** (2001) 182002.
[11] Jlab Hall A Collaboration, C. Muñoz Camancho *et al.*, Phys. Rev. Lett. **97** (2006) 262002.
[12] HERMES Collaboration, A. Airapetian *et al.*, Phys. Rev. **D75** (2007) 011103(R).
[13] A. Bacchetta *et al.*, Phys. Rev. **D70** (2004) 117504.
[14] M. Diehl, T. Gousset, B. Pire and J. P. Ralston, Phys. Lett. **B411** (1997) 193.
[15] A.V. Belitsky, D. Müller and A. Kirchner, Nucl. Phys. **B629** (2002) 323.
[16] F. Ellinghaus, W.-D. Nowak, A.V. Vinnikov and Z. Ye, Eur. Phys. J. **C46** (2006) 729.
[17] HERMES Collaboration (M. Kopytin for the collaboration). Proceedings of the 13th International Workshop on Deep Inelastic Scattering, Madison, USA, 2005, AIP Conf. Proc. 792 (2005) 424.
[18] CLAS Collaboration, S. Chen *et al.*, Phys. Rev. Lett. **97** (2006) 072002.
[19] M. Diehl, Eur. Phys. J. **C19** (2001) 485.
[20] A. V. Belitsky and D. Müller, Phys. Lett. **B486** (2000) 369.
[21] N. Kivel and L. Mankiewicz, Eur. Phys. J. **C21** (2001) 621.
[22] HERMES Collaboration, A. Airapetian *et al.*, Nucl. Instr. and Meth. **A540** (2005) 68.
[23] HERMES Collaboration, K. Ackerstaff *et al.*, Nucl. Instr. and Meth. **A417** (1998) 230.
[24] F. Ellinghaus, PhD thesis, Humboldt University Berlin, Germany, January 2004, DESY-THESIS-2004-005.
[25] B. Krauss, PhD thesis, Physikalisches Institut II, FAU Erlangen-Nürnberg, February 2005.

[26] L.W. Mo and Y.S. Tsai, Rev. Mod. Phys. **41** (1969) 205.
[27] F.W. Brasse *et al.*, Nucl. Phys. **B110** (1976) 413.
[28] D. Drechsel *et al.*, Nucl. Phys. **A645** (1999) 145.
[29] G. Ingelman, A. Edin and J. Rathsman, Comput. Phys. Commun. **101** (1997) 108.
[30] T. Sjöstrand, Comput. Phys. Commun. **82** (1994) 74.
[31] A. Hillenbrand, PhD thesis, University Erlangen–Nuremberg, Germany, November 2005, DESY-THESIS-2005-035.
[32] M. Vanderhaeghen, P.A.M. Guichon and M. Guidal, Phys. Rev. **D60** (1999) 094017.
[33] M. Vanderhaeghen *et al.*, Phys. Rev. **C62** (2000) 025501.
[34] Z. Ye, PhD thesis, University Hamburg, Germany, December 2006, DESY-THESIS-2007-005.
[35] M. Diehl and S. Sapeta, Eur. Phys. J. **C41** (2005) 515.
[36] R. Barlow, Nucl. Instr. and Meth. **A297** (1990) 496.
[37] V.A. Korotkov and W.-D. Nowak, Eur. Phys. J. **C23** (2002) 455.
[38] A.V. Afanasev, M.I. Konchatnij and N.P. Merenkov, J. Exp. Theor. Phys. **102** (2006) 220.
[39] K. Goeke, M.V. Polyakov and M. Vanderhaeghen, Prog. Part. Nucl. Phys. **47** (2001) 401.
[40] A.V. Radyushkin, Phys. Rev. **D59** (1999) 014030; Phys. Lett. **B449** (1999) 81.
[41] A.D. Martin *et al.*, Eur. Phys. J. **C4** (1998) 463.
[42] I.V. Musatov and A.V. Radyushkin, Phys. Rev. **D61** (2000) 074027.
[43] M.V. Polyakov and C. Weiss, Phys. Rev. **D60** (1999) 114017.
[44] V.Y. Petrov *et al.*, Phys. Rev. **D57** (1998) 4325.
[45] M. Vanderhaeghen, P.A.M. Guichon and M. Guidal, Computer code for the calculation of DVCS and BH processes in the reaction $e\,p \to e'\,p'\,\gamma$, Priv. Comm., 2001.
[46] QCDSF/UKQCD Collaboration, M. Göckeler *et al.*, Eur. Phys. J. **A32** (2007) 445.
[47] LHPC Collaboration, Ph. Hägler *et al.*, arXiv:0705.4295 [hep-lat].
[48] M.V. Polyakov and A.G. Shuvaev, arXiv: hep-ph/0207153.
[49] V. Guzey and T. Teckentrup, Phys. Rev. **D74** (2006) 054027.
[50] V. Guzey and T. Teckentrup, Priv. Comm., 2007.
[51] F. Ellinghaus, Proceedings of the Workshop on "Exclusive Processes at High Momentum Transfer", Newport News, Virginia, USA, May 2007; arXiv:0710.5768 [hep-ex]
[52] Q. M. Ohtani *et al.*[QCDSF-UKQCD Collaboration], arXiv:0710.1534 [hep-lat].
[53] M. Diehl, T. Feldmann, R. Jakob, P. Kroll, Eur. Phys. J. **C39** (2005) 1.
[54] P. Kroll, Proceedings of the Workshop on "Exclusive Processes at High Momentum Transfer", Newport News, Virginia, USA, May 2007; arXiv:0710.2771 [hep-ph].
[55] JLab Hall A Collaboration, M. Mazouz et al., Phys. Rev. Lett. **99** (2007) 242501.